Layer-dependent surface potential of phosphorene and anisotropic/layer-dependent charge transfer in phosphorene-gold hybrid system

Renjing Xu,[1] Jiong Yang,[1] Yi Zhu, [1] Yan Han,[1] Jiajie Pei,[1,2] Ye Win Myint,[1] Shuang Zhang,[1] and Yuerui Lu[1*]

[1]Research School of Engineering, College of Engineering and Computer Science, the Australian National University, Canberra, ACT, 0200, Australia

[2]School of Mechanical Engineering, Beijing Institute of Technology, Beijing, 100081, China

* To whom correspondence should be addressed: Yuerui Lu (yuerui.lu@anu.edu.au)

ABSTRACT: The surface potential and the efficiency of interfacial charge transfer are extremely important for designing future semiconductor devices based on the emerging two-dimensional (2D) phosphorene. Here, we directly measured the strongly layer-dependent surface potential of mono- and few-layer phosphorene on gold, which confirms with the reported theoretical prediction. At the same time, we used an optical way - photoluminescence (PL) spectroscopy to probe the charge transfer in phosphorene-gold hybrid system. We firstly observed highly anisotropic and layer-dependent PL quenching in the phosphorene-gold hybrid system, which is attributed to the highly anisotropic/layer-dependent interfacial charge transfer.

Keywords: Surface potential, phosphorene, charge transfer, quenching

Phosphorene, a new family member of two-dimensional (2D) layered materials, has attracted tremendous attention owing to its unique anisotropic manner[1-6], layer-dependent photoluminescence[7, 8], and quasi-one-dimensional (1D) excitonic nature[9, 10], which are all in drastic contrast with the properties of other 2D materials, such as graphene[11] and transition metal dichalcogenide (TMD) semiconductors[12-15]. Particularly, phosphorene with narrow band gaps ranging from mid-infrared to near-infrared wavelengths can fill the space between the gapless graphene and the comparably large gap TMD semiconductors, leading to many new electronic and optoelectronic devices[1-10], including field effect transistors, sensors, light emitting diodes, solar cells and so on. All these devices involve the photon-to-electron or electron-to-photon conversions, in which the interfacial charge transfer plays an important factor[16-18]. Up to date, the important properties of metal-phosphorene interfaces are still underexplored, including the direct measurement of the surface potential of phosphorene, the interfacial charge transfer in the phosphorene-metal hybrid system, etc.

RESULTS AND DISCUSSION

In this work, we directly measured the surface potential of mono- and few-layer phosphorene on gold substrate by Kelvin probe force microscope (KPFM). The measured surface potential shows strong layer dependence, which is consistent with reported theoretical prediction[19]. At the same time, we used photoluminescence (PL) spectroscopy to probe the charge transfer in phosphorene-gold hybrid system. We firstly observed highly anisotropic and layer-dependent PL quenching, which is attributed to the highly anisotropic/layer-dependent interfacial charge transfer in the phosphorene-gold hybrid system. Our results provide very useful information

for heterostructure device design and pave new avenues for future new optoelectronic devices using phosphorene.

Surface potential, also known as work function, is very important for semiconductor devices, since it determines the interfacial energy barrier and thus the efficiency of carrier injections in electronic and optoelectronic devices. Here, a powerful tool KPFM was used to directly measure the surface potential of mono- and few-layer phosphorene flakes on gold substrates (Figure 1). In experiments, mono- and few-layer phosphorene flakes were mechanical exfoliated onto gold substrates. The thin layers were firstly identified by the contrast under optical microscope (Figure 1b) and the layer numbers were then quickly and precisely determined by our recently developed technique phase-shifting interferometer[20] (Figure 1c and 1d, Figure S1). The layer number was also confirmed by the measured PL spectra[20]. For the surface potential measurements, we applied an AC modulation voltage and a DC bias voltage between the sample and the tip (Figure 1a). The resulting electrostatic forces acting on the tip were detected by using a lock-in technique to analyze the amplitude of the tip's oscillation in the KPFM system. The amplitude signal includes the DC bias voltage plus the work function difference between the tip and the sample. The compensated DC voltage signal, controlled by a feedback circuit, corresponds to the local surface potential of the sample surface[21, 22]. The resulting KPFM image (Figure 1e) maps the variation of the surface potential. From this KPFM image, we could determine the surface potential difference between the gold substrate and the phosphorene flake, defined as $\phi_{Au} - \phi_{BP}$, where ϕ_{Au} and ϕ_{BP} are the work functions of gold and phosphorene flake, respectively. The measured statistical surface potential differences

for mono-layer (1L) to five-layer (5L) phosphorene and thick flakes (relative to gold surface) are 514 ± 15, 536 ± 6, 555 ± 7, 599 ± 14, 665 ± 21 and 693 ± 10 meV, respectively, which is consistent with the trend of previous simulated results[19]. The KPFM measurements were all completed within 40 minutes after phosphorene exfoliation to minimize the influence from sample degradation.

The layer-dependent surface potential of the phosphorene can enable the engineering of the exciton dynamics in the phosphorene-metal heterostructures, including generation, dissociation, transfer, and recombination, which bears tremendous significance for fundamental and applied interests[18, 23]. Here, we study charge transfer dynamics in phsophorene-gold hybrid system using PL spectroscopy (Figure 2), which has been used to probe the charge transfer in TMD 2D semiconductor heterostructures[16-18, 24]. In our experiment, few-layer phosphorene flakes were mechanically exfoliated and transferred onto the edge of a gold pad, which was prepatterned onto a SiO_2/Si (275 nm thermal oxide substrate) substrate. The transfer process was carefully carried out to make sure half of the few-layer phosphorene flake lays on the SiO_2/Si substrate whilst the other half is on the gold (Figure 2a and 2b), which will give us precise comparison of the PL emissions from these two halves. From the optical microscope image (Figure 2b), the first half of the few-layer phosphorene sample on the SiO_2/Si substrate presents much larger contrast than the other half on the gold, which is because the thickness of the SiO_2 was pre-designed for the best contrast[25]. The layer number was precisely determined by phase-shift interferometry (PSI) (Figure 2c & 2d, Figure S2 & S3), which has been demonstrated to be a fast and precise way to identify the layer number of phosphorene in our

previous report[26]. The layer number identification was also confirmed by comparing the

measured PL spectra with our previous reports[8, 26]. Figure 2e shows the measured PL spectra

of the bilayer phosphorene samples on both gold and SiO_2/Si substrate, using a 532 nm

Nd:YAG laser as the excitation source. The PL intensity of the main peak at 945 nm from the

2L phosphorene on Au is much lower than that from the second half of 2L phosphorene on

SiO_2/Si substrate, which means the Au substrate leads to significantly PL quenching. This PL

quenching is due to the fast interfacial charge transfer between the gold and the 2L phosphorene

sample. From the energy diagram shown in Figure 2f, the photo-excited holes are attracted

towards the Au-phosphorene interface and then annihilated by the electrons from the gold[27].

Hence, as the consequence of the fast charge transfer, the radioactive recombination will be

eliminated, leading to the PL quenching in the phosphorene-gold hybrid system.

In order to fabricate high-efficiency solar cells based on phosphorene, it is very important to

optimize the charge transfer efficiency and thus the carrier collection efficiency in the

phosphorene-metal hybrid system[18, 28]. Owing to the unique puckered structure, phosphorene

has been demonstrated to show highly anisotropic properties, such as highly anisotropic

excitons[9, 29], carrier mobility[30], carrier effective masses[17, 30], thermal expansion coefficient[31]

and shear factor[31], which are all in drastic contrast with the properties of graphene[11] and TMD

semiconductors[12-14]. Therefore, an anisotropic charge transfer in the phosphorene-gold hybrid

system could be expected, which makes it more critical to precisely determine the right

orientation for the optimized charge transfer. Here, we used the angle-resolved PL quenching

measurements to characterize the anisotropic charge transfer in the phosphorene-gold hybrid

system. In the setup of the angle-resolved PL measurement, a linearly polarized Nd:YAG laser

with a wavelength of 532 nm was used as the excitation source. The polarization angle of the

incident light is controlled by an angle-variable half-wave plate. The polarization angle of the

PL emission (θ) is characterized by inserting an angle-variable polarizer in front of the detector.

We firstly used the excitation polarization dependent PL measurements to determine the

crystalline orientation of the 2L phosphorene flake on SiO_2/Si substrate[10]. Then the armchair

direction is selected as the zero-degree reference for θ (Figure 3a, inset). Next, we measured

the polarization dependence of the PL emission by fixing the excitation polarization along the

armchair direction. Figure 3a presents the polarization dependent PL emission from the first

half of the 2L phosphorene flake on SiO_2/Si substrate (Figure 2b). The red fitting curve shows

that the PL intensity follows sinusoid with period of $\sim 180^o$. The PL intensity reaches its

maximum at $\theta = 0^o$ (armchair direction) and its minimum at $\theta = 90^o$ (zigzag direction),

which is consistent with our previous report[10]. The measured PL emission from the second half

of the 2L phophorene flake on Au (Figure 3b) is also linearly polarized, whereas its maximum

PL intensity appears at $\theta = 50^o$ instead of 0°. We attribute this angle difference to be caused

by the anisotropic interfacial charge transfer between the phosphorene and gold. Here we use

a quenching factor, which is defined by $\frac{\text{PL intensity on } SiO_2/Si}{\text{PL intensity on Au}}$, to characterize the charge transfer.

Figure 3c shows the measured quenching factor as a function of the emission polarization angle.

The quenching factor is strongly dependent on the polarization angle, which can be fitted by a

sinusoidal curve with a period of $\sim 180^o$. The measured maximum quenching factor was 6,

which occurs at $\theta = 0^o$, while the minimum quenching factor is 1.5, which occurs at $\theta = 90^o$. This strongly anisotropic PL quenching can be understood by the anisotropic interfacial

charge transfer between the phosphorene and gold. Since the PL quenching effect between the semiconductor materials and metal is basically due to the transport of photo-excited charges[24, 27]. Phosphorene has the maximum charge mobility along the armchair direction[32], which leads to the maximum speed of charge transfer and thus the maximum quenching factor along the armchair direction.

Besides the charge mobility discussed above, the Schottky energy barrier is another important factor to determine the efficiency of interfacial charge transfer[17, 18]. Previous calculations have predicted that phosphorene owns layer-dependent band alignment and there is a significant shift of valence band edge upon thickness variation, which can be useful for tuning Schottky barrier to promote hole injection efficiency[33]. This prediction is confirmed from our following layer-dependent PL quenching experiments in the phosphorene-gold hybrid system. The measured quenching factor of a 3L phosphorene on Au is around one order of magnitude higher than that of a 2L phosphorene, for emission polarization of both zigzag and armchair directions (Figure 4a), respectively. This strongly layer-dependent PL quenching in phosphorene is in great contrast with that in MoS_2, where the quenching factor does not make large changes for mono- and few-layer MoS_2[24]. The layer-dependent PL quenching in phosphorene-gold hybrid system can be understood from their band diagrams, as shown in Figure 4b. The band diagrams were generated based on the calculated valence band maximum (VBM) and conduction band minimum (CBM) for few-layer phosphorene[19] and our measured surface potential difference between phosphorene and Au. As shown in Figure 1f, the measured surface potential difference between 3L phsophorene and gold (~555 meV) is larger than that for 2L phosphorene (~536

meV), which results in larger Schottky barrier for 3L phosphorene-Au hybrid system than that for 2L phosphorene (Figure 4b). This larger Schottky barrier will increase the force to pull holes towards the phosphorene-gold interface, leading to more efficient interfacial charge transfer and thus much larger PL quenching for 3L than 2L phosphorene in the phosphorene-gold hybrid system.

CONCLUSIONS

In conclusion, we directly measured the layer-dependent surface potential of mono- and few-layer phosphorene on gold substrate, which is consistent with reported theoretical prediction[19]. At the same time, we used an optical way - PL spectroscopy to probe the charge transfer in phosphorene-gold hybrid system. We firstly observed highly anisotropic and layer-dependent PL quenching, which is attributed to the highly anisotropic/layer-dependent interfacial charge transfer in the phosphorene-gold hybrid system. Our results open the door for **designing** future electronic and optoelectronic heterostructure devices using phosphorene.

EXPERIMENTAL METHODS

We used mechanical exfoliation to transfer[34] a phosphorene flake onto the edge a pre-patterned gold electrode on a SiO_2/Si substrate (275 nm thermal oxide on n^+-doped silicon). The gold electrodes were patterned by conventional photolithography, metal deposition, and lift-off processes. All PL and polarization measurements were conducted using a T64000 micro-Raman system equipped with a charge-coupled device (CCD) and InGaAs detectors, along with a 532nm Nd:YAG laser as the excitation source. Subsequent to PSI measurement, the

sample was placed into a Linkam THMS 600 chamber, with a slow flow of nitrogen gas to prevent degradation of the sample[8]. To avoid laser-induced sample damage, all PL spectra were recorded at low power levels: P ~ 20 µW. The surface potential was measured by KPFM. The model of the KPFM used in the experiments was Bruker Multimode VIII with Peak Force TUNA.

Competing financial interests

The authors declare that they have no competing financial interests.

Supporting Information Available: Details of theoretical calculation methods, more experimental measurement results and data analysis, are shown in Supporting Information.

References

1. H. Liu, A. T. Neal, Z. Zhu, Z. Luo, X. Xu, D. Tománek and P. D. Ye, *ACS Nano*, 2014, 8, 4033-4041.
2. M. Buscema, D. J. Groenendijk, S. I. Blanter, G. A. Steele, H. S. J. van der Zant and A. Castellanos-Gomez, *Nano Lett.*, 2014, 14, 3347-3352.
3. R. Fei and L. Yang, *Nano Lett.*, 2014, 14, 2884-2889.
4. F. Xia, H. Wang and Y. Jia, *Nat. Commun.*, 2014, 5.
5. L. Li, Y. Yu, G. J. Ye, Q. Ge, X. Ou, H. Wu, D. Feng, X. H. Chen and Y. Zhang, *Nat. Nanotechnol.*, 2014, 9, 372-377.
6. T. Hong, B. Chamlagain, W. Lin, H.-J. Chuang, M. Pan, Z. Zhou and Y.-Q. Xu, *Nanoscale*, 2014, 6, 8978-8983.
7. J. Qiao, X. Kong, Z.-X. Hu, F. Yang and W. Ji, *Nat. Commun.*, 2014, 5.
8. S. Zhang, J. Yang, R. Xu, F. Wang, W. Li, M. Ghufran, Y.-W. Zhang, Z. Yu, G. Zhang, Q. Qin and Y. Lu, *ACS Nano*, 2014, 8, 9590-9596.
9. V. Tran, R. Soklaski, Y. Liang and L. Yang, *Phys. Rev. B*, 2014, 89, 235319.
10. S. Zhang, R. Xu, F. Wang, J. Yang, Z. Wang, J. Pei, Y. W. Myint, B. Xing, Z. Yu, L. Fu, Q. Qin and Y. Lu, *arXiv:1411.6124*, 2014, DOI: arXiv:1411.6124.
11. A. K. Geim and K. S. Novoselov, *Nat. Mater.*, 2007, 6, 183-191.
12. B. Radisavljevic, A. Radenovic, J. Brivio, V. Giacometti and A. Kis, *Nat. Nanotechnol.*, 2011, 6, 147-150.
13. K. F. Mak, K. He, C. Lee, G. H. Lee, J. Hone, T. F. Heinz and J. Shan, *Nat. Mater.*, 2013, 12, 207-211.
14. J. S. Ross, S. Wu, H. Yu, N. J. Ghimire, A. M. Jones, G. Aivazian, J. Yan, D. G. Mandrus, D. Xiao, W. Yao and X. Xu, *Nat. Commun.*, 2013, 4, 1474.
15. J. Yang, T. Lü, Y. W. Myint, J. Pei, D. Macdonald, J.-C. Zheng and Y. Lu, *ACS Nano*, 2015, 9, 6603-6609.
16. J. Yuan, S. Najmaei, Z. Zhang, J. Zhang, S. Lei, P. M. Ajayan, B. I. Yakobson and J. Lou, *ACS Nano*, 2015, 9, 555-563.
17. X. Hong, J. Kim, S.-F. Shi, Y. Zhang, C. Jin, Y. Sun, S. Tongay, J. Wu, Y. Zhang and F. Wang, *Nat. Nanotechnol.*, 2014, 9, 682-686.
18. Y. Yu, S. Hu, L. Su, L. Huang, Y. Liu, Z. Jin, A. A. Purezky, D. B. Geohegan, K. W. Kim, Y. Zhang and L. Cao, *Nano Lett.*, 2015, 15, 486-491.
19. Y. Cai, G. Zhang and Y.-W. Zhang, *Sci. Rep.*, 2014, 4.
20. J. Yang, R. Xu, J. Pei, Y. W. Myint, F. Wang, Z. Wang, S. Zhang, Z. Yu and Y. Lu, *Light Sci Appl*, 2015, 4, e312.
21. M. Nonnenmacher, M. P. O'Boyle and H. K. Wickramasinghe, *Appl. Phys. Lett.*, 1991, 58, 2921-2923.
22. Y. Li, C.-Y. Xu and L. Zhen, *Appl. Phys. Lett.*, 2013, 102, 143110.
23. S. Das, W. Zhang, M. Demarteau, A. Hoffmann, M. Dubey and A. Roelofs, *Nano Lett.*, 2014, 14, 5733-5739.
24. U. Bhanu, M. R. Islam, L. Tetard and S. I. Khondaker, *Sci. Rep.*, 2014, 4.
25. M. Benameur, B. Radisavljevic, J. Heron, S. Sahoo, H. Berger and A. Kis, *Nanotechnology*, 2011, 22, 125706.
26. J. Yang, R. Xu, J. Pei, Y. W. Myint, F. Wang, Z. Wang, S. Zhang, Z. Yu and Y. Lu,

arXiv:1504.06386v2, 2015, DOI: arXiv:1504.06386v2.

27. Z. Yin, H. Li, H. Li, L. Jiang, Y. Shi, Y. Sun, G. Lu, Q. Zhang, X. Chen and H. Zhang, *ACS Nano*, 2012, 6, 74-80.

28. M.-L. Tsai, S.-H. Su, J.-K. Chang, D.-S. Tsai, C.-H. Chen, C.-I. Wu, L.-J. Li, L.-J. Chen and J.-H. He, *ACS Nano*, 2014, 8, 8317-8322.

29. X. Wang, A. M. Jones, K. L. Seyler, V. Tran, Y. Jia, H. Zhao, H. Wang, L. Yang, X. Xu and F. Xia, *arXiv preprint arXiv:1411.1695*, 2014.

30. J. Qiao, X. Kong, Z.-X. Hu, F. Yang and W. Ji, *Nature communications*, 2014, 5.

31. S. Appalakondaiah, G. Vaitheeswaran, S. Lebegue, N. E. Christensen and A. Svane, *Physical Review B*, 2012, 86, 035105.

32. Y. Deng, Z. Luo, N. J. Conrad, H. Liu, Y. Gong, S. Najmaei, P. M. Ajayan, J. Lou, X. Xu and P. D. Ye, *ACS Nano*, 2014, 8, 8292-8299.

33. K. H. Li, LiuX, WangQ, ZhaoS and MiZ, *Nat. Nanotechnol.*, 2015, 10, 140-144.

34. A. Castellanos-Gomez, M. Buscema, R. Molenaar, V. Singh, L. Janssen, H. S. J. v. d. Zant and G. A. Steele, *2D Materials*, 2014, 1, 011002.

FIGURE CAPTIONS

Figure 1 | Measured surface potential of mono- and few-layer phosphorene by Kelvin probe force microscope (KPFM). a, Schematic plot of KPFM measurement. **b**, Optical microscope image of the sample with two- and three-layer (2L and 3L) phosphorene on gold substrate. **c**, Phase-shifting interferometry (PSI) image of the 2L and 3L phosphorene from the box enclosed by the dash line in **(b)**. **d**, PSI measured optical path length (OPL) values versus scan position for 2L and 3L phosphorene (or black phosphorous, shorted as BP) along the dash line in **(c)**. The measured optical path length (OPL) values of the sample on gold are 6.2 and 9.4 nm, indicating bi- and tri-layer, respectively (Figure S1). **e**, Surface potential contour image of the dashed line box region in **(b)**, measured by KPFM. The surface potential differences between the gold substrate and the phosphorene layers (2L and 3L) are also shown, respectively. The surface potential difference between the gold substrate and the phosphorene flake is defined as $\phi_{Au} - \phi_{BP}$, where ϕ_{Au} and ϕ_{BP} are the work functions of gold and phosphorene flake, respectively. **f**, Measured layer-dependent surface potential differences between the gold substrate and phosphorene flakes. The error bar represents the statistical measurement variations from at least two samples for each layer number.

Figure 2 | Photoluminescence (PL) quenching in phosphorene-gold hybrid system. a, Schematic plot of the device structure. A few-layer phosphorene flake was mechanically exfoliated and dryly transferred onto the edge of a gold pad, which was pre-patterned onto a SiO$_2$/Si (275 nm thermal oxide substrate) substrate. The transfer process was carefully carried out to make sure half of the few-layer phosphorene flake lays on the SiO$_2$/Si substrate whilst the other half is on the gold, which will give us precise comparison of the PL emissions from

these two regions. **b**, Optical microscope image of the mechanically transferred few-layer phosphorene flakes, with half on gold and half on SiO_2. **c**, PSI image of phosphorene samples from the lower box on SiO_2/Si substrate enclosed by the dash line in (**b**). **d**, PSI measured OPL values versus scan position for the phosphorene along the dash line in (**c**). **e**, Measured PL spectra from the 2L phosphorene on Au and SiO_2/Si substrate, with the background PL spectra for comparison. **f**, Schematic plot of the band diagram, showing the mechanism of the PL quenching in phosphorene-gold hybrid system.

Figure 3 | Anisotropic PL quenching/charge transfer in phosphorene-gold hybrid system. a-b, Measured PL peak intensities as a function of the emission polarization angle θ, from the 2L phosphorene sample half on SiO_2/Si **(a)** and the second half on gold **(b)**, respectively.   The red lines are the fitted sinusoidal curves. Inset: Schematic plot of the top view of phosphorene lattice structure and coordinates for polarization angle θ. **c**, The measured PL quenching factor from the 2L phosphorene sample, as a function of the emission polarization angle. Quenching factor is defined by $\frac{\text{PL intensity on } SiO_2/Si}{\text{PL intensity on Au}}$. The red line is the fitted sinusoidal curve.

Figure 4 | Layer-dependent PL quenching/charge transfer in phosphorene-gold hybrid system. a, Measured PL quenching factors from 2L and 3L phosphorene samples, with emission polarization angles along the armchair and zigzag directions, respectively. The error bar represents the statistical measurement variation from at least two samples. **b**, Schematic plot of the band diagrams for 2L and 3L phosphorene-gold hybrid systems. The band diagrams were generated based on the calculated valence band maximum (VBM) and conduction band minimum (CBM) for few-layer phosphorene[19] and our measured surface potential difference between phosphorene and Au.
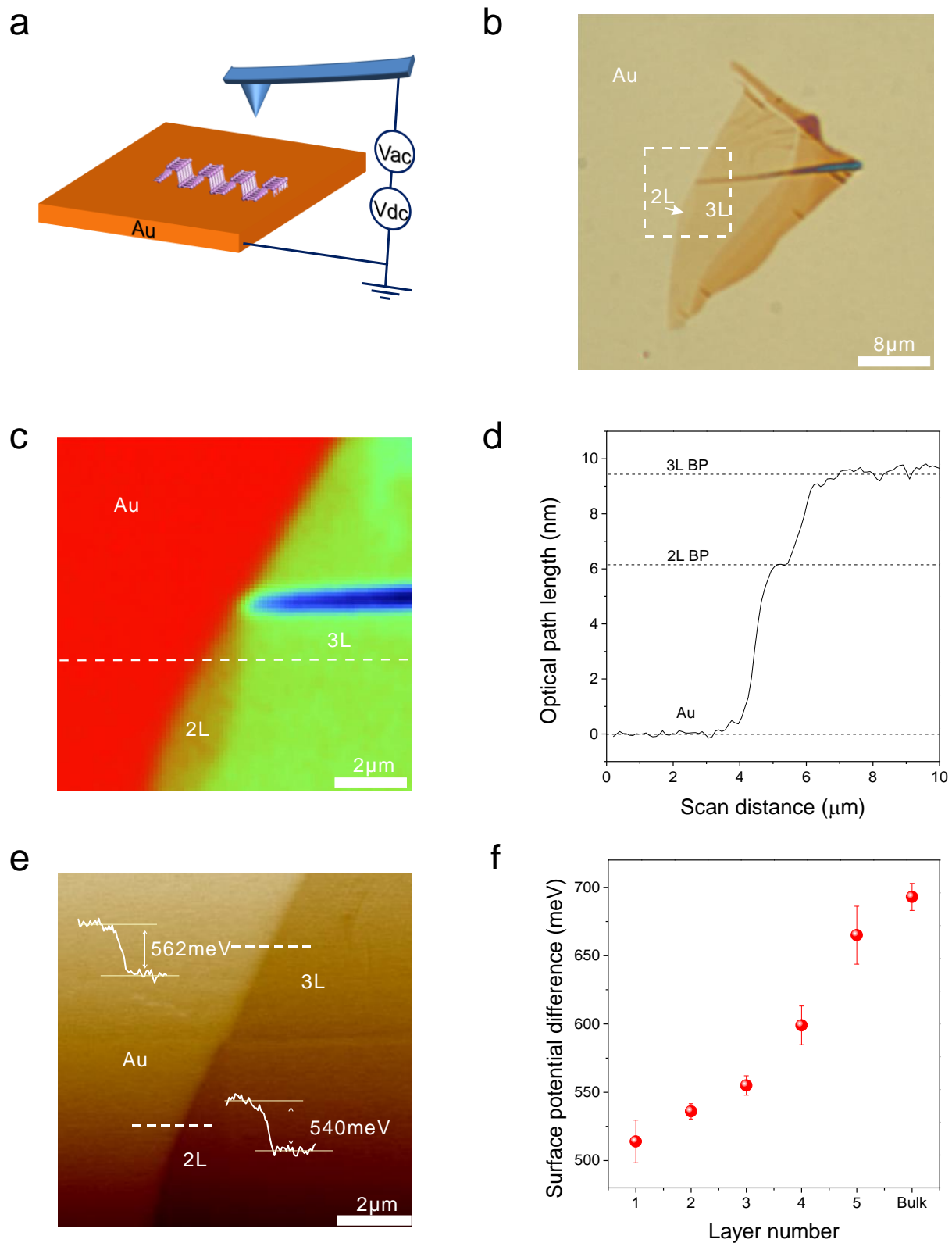
a

b

Au

2L 3L

8μm

c

Au

3L

2L

2μm

d

3L BP

2L BP
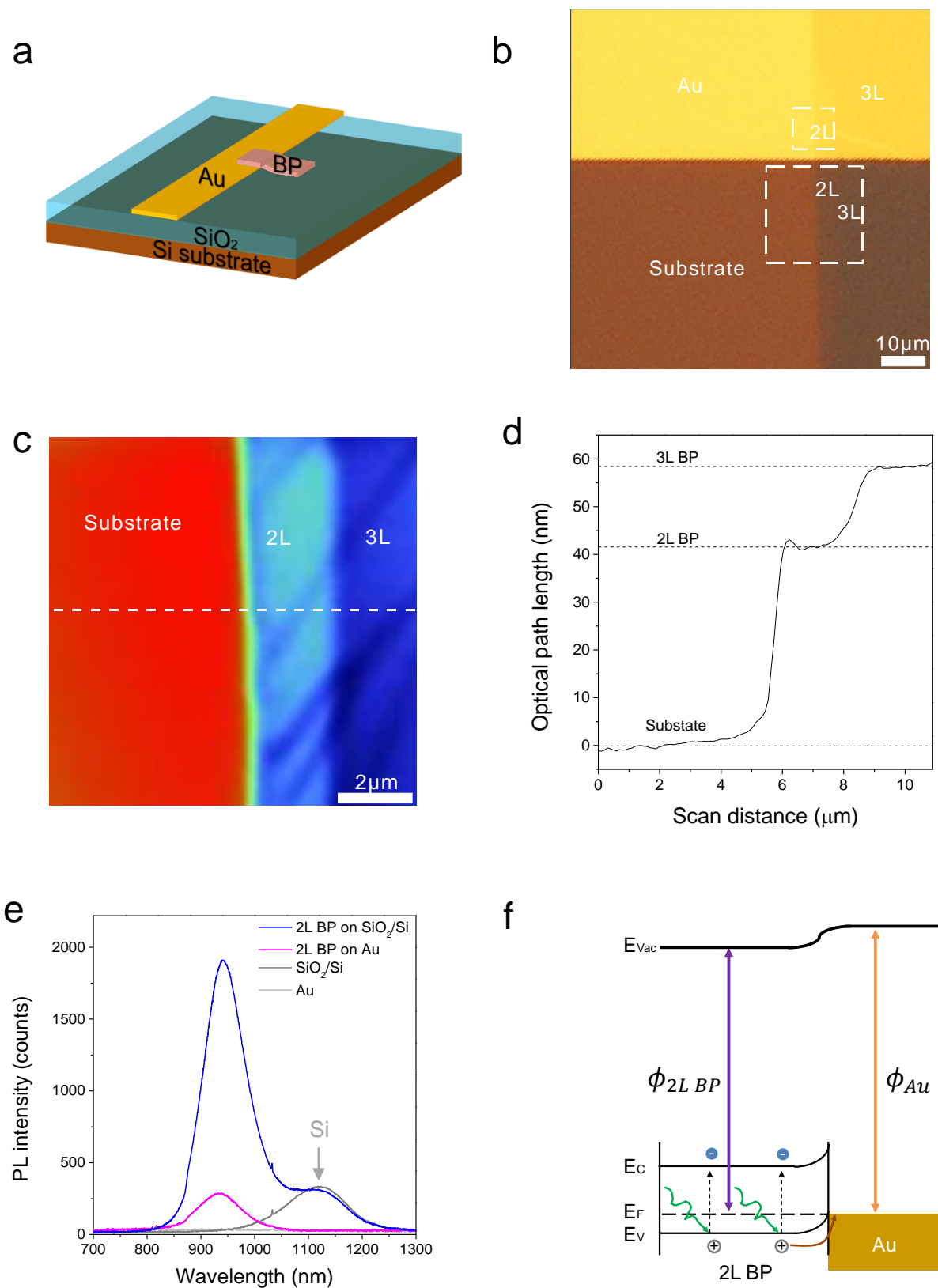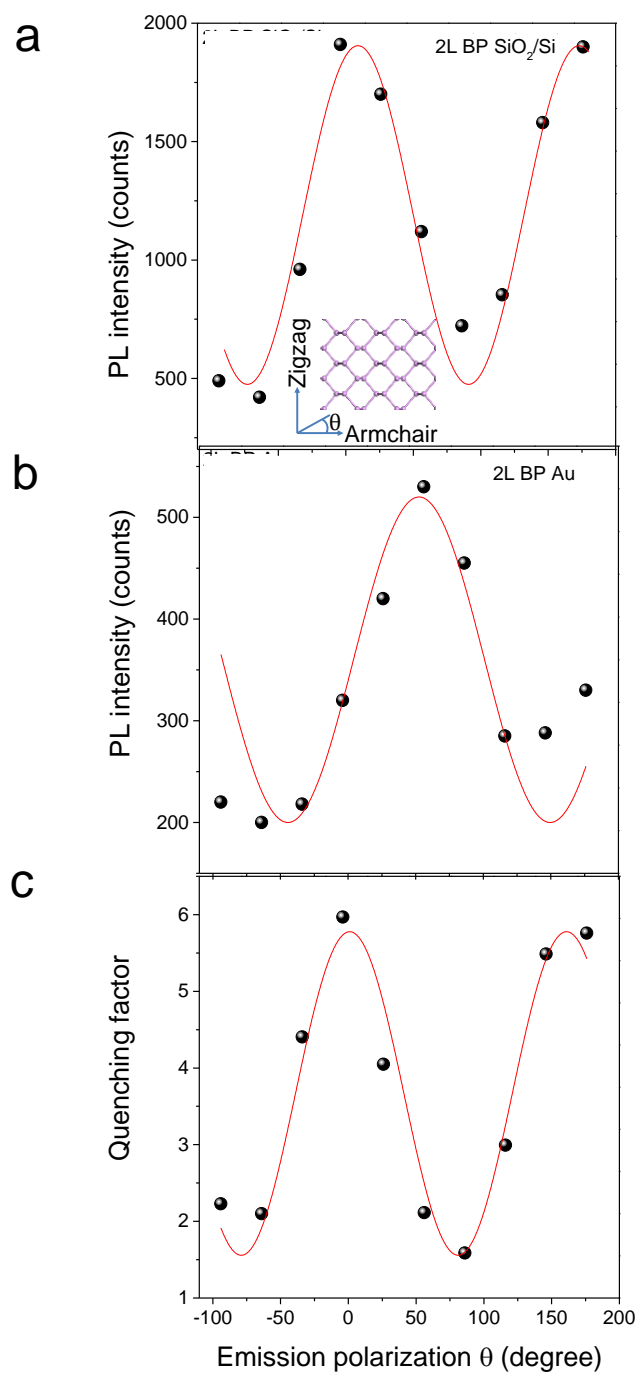
Au

e

562meV

3L

Au

2L

540meV

2μm

f

Figure 1

a

b

c

d

e

f

Figure 2

Figure 3

Figure 4